LEAD PRESSURE LOSS IN THE HEAT EXCHANGER OF THE ELSY FAST LEAD-COOLED REACTOR BY CFD APPROACH

Alexandru Onea, Michael Böttcher, Dankward Struwe

Karlsruhe Institute of Technology (KIT), Institute for Neutron Physics and Reactor Technology, Hermann-von-Helmholtz-Platz 1, 76344 Eggenstein-Leopoldshafen, Germany

Abstract

The present paper discusses the pressure loss through the spiral heat exchanger (HX) proposed in the ELSY (European-Lead cooled SYstem) project. An approach based on CFD (Computational Fluid Dynamics) using the commercial code ANSYS CFX has been used for exploring the flow through the HX. The HX consists of perforated double inner and double outer walls, as well as an innovative spiral design of the pipe bundle. Two investigation ways are considered, namely a detailed local approach by employing unit slice models and a simplified global approach. The unit slice models discretize accurately small parts of the HX, while the global models consider geometrical simplifications of the main HX components. ANSYS CFX was qualified for pressure loss simulations through perforated plates. At nominal conditions, the pressure loss estimated meets the requirements issued in the reactor design.

1. INTRODUCTION

The nuclear reactor ELSY is a project for a fast lead-cooled reactor, developed within the 6th European Framework Programme of EURATOM (Alemberti et al., 2009). The Italian company Ansaldo Nucleare coordinated the project, in which a consortium of 19 participants took part.

The ELSY project is a 600MWe pool-type reactor. It aims to demonstrate the feasibility of a lead-cooled fast critical reactor for generation of electricity, the identification of solutions for a reduced volume of the primary system and for simplified reactor internals. The project aims to comply with the requirements of the IVth generation of nuclear power plants.

The reactor is designed to burn its own minor actinides (MA) and to be self-sustaining in plutonium.

For the plant layout, the simplicity, the economics, and safety were the main design criteria. Therefore, a compact reactor vessel (RV) is proposed, while all internal components are designed to be removable. As a safety-by-design measure, it is desired that the overall lead pressure loss through the primary circuit would allow the decay heat removal by natural circulation in case of planned or unplanned reactor shutdown. For this purpose, the knowledge of the lead pressure loss in every component of the primary side is mandatory. The task of the present paper is the discussion of the lead pressure loss through the heat exchanger.

We employed the commercial CFD code ANSYS CFX to investigate the flow of lead through the heat exchanger. The heat exchanger has the smallest relevant length scale in the millimetre range and the longest relevant length scale in the meter range. This inhibits the construction of a detailed CFD model of the entire reactor with today's computational resources. Therefore, the first approach considered (Onea et al., 2010) focuses on determining the pressure loss using detailed unit slice models that consider only small parts of the reactor. These results are further used in this paper for the setup of unit slice models that consider all major components (the lateral walls and the pipe bundle) and for the setup of a simplified complete model. The pressure losses determined were further employed in a global CFD thermo-dynamic analysis of the ELSY reactor by Böttcher and Onea (2010).

The ELSY HX distinguishes itself through the innovative design of its pipe bundle, which consists of tubes arranged in a staggered way. In comparison to a conventional U or J-type arrangement, the possible advantages brought by a spiral pipe arrangement are reduced volume, lower pressure loss, higher resistance to thermal loads and reduced number of pipes. The cross flow through such a pipe bundle is fluctuating due to the periodic generation of vortices. Shedding of these vortices on the tubes

causes them to vibrate, i.e. the mechanical stresses generated on the tubes have the potential to cause them mechanically to fail. Even a steady flow through a pipe bundle can cause vibrations of the tubes in a heat exchanger, resulting in flow fluctuations, as discussed by Blevins (1977). These flow-induced vibrations are due to the jet switching - which is a result of the coupling and uncoupling of the fluid jets behind the tube array - and due to the interaction of the tubes with the wake of the upstream tubes. Within the study no model has been deemed for the vibration of the tubes, therefore the flow-induced vibration, which causes flow instabilities, can be ruled out as a possible reason for the flow unsteadiness.

Iwaki et al. (2004) used particle image velocimetry to determine experimentally the characteristics of the flow through a staggered pipe bundle. They report three kinds of flow regions, namely the vortex, the converging, and the diverging regions, designated as X-type flow by other authors. A stable, similar, and symmetric pair of vortices is observed behind all tubes. The flow exhibits a strong non-uniform character only in the region of the last pipe rows. Oscillations of the axial flow between vertical neighbouring tubes were observed in that region. Behind the second row of pipes, the vorticity magnitude decreases to about half the value behind first row and steady afterwards.

Aiba et al. (1982) report experimental results for two staggered pipe arrangements. Different flow behaviours are observed, due to the differences in the geometric arrangement. The tightest pipe arrangement exhibits non-uniform flow characteristics with large velocity fluctuations, while the flow is smoother for the second, larger spaced, pipe array considered. Therefore, for the first pipe array, the drag has a larger magnitude and oscillates for the first rows in comparison to the almost constant drag determined for the second case.

In the experiments performed by Simonin and Barcouda (1988), the measurements indicate that the flow instabilities decrease after the forth row of the pipe bundle, which consists of seven layers of cylinders, displaced in a staggered way. It is found that in the wakes of the tubes, regions of low velocity and high turbulent intensity are developing. The turbulence level rises after the first row, reaches a maximum at the second row and decreases to a rather constant value afterwards. A strong anisotropy of the turbulent kinetic energy is observed. The Reynolds number in these experiments, based on the cylinder hydraulic diameter and inlet velocity is about 18000. Based on the flow steadiness reported, several numerical studies considered only a small part of the passage between tubes, by employing periodic boundary conditions (Rollet-Miet et al.; 1999, Kuehlert et al.; 2008, Benhamadouche and Laurence; 2003). Rollet-Miet et al. (1999) report good agreement with the experiment for the Large Eddy Simulation (LES) approach, since the size of the large vortices equals the size of the tubes. Limitations are reported for the Reynolds Averaged Navier Stokes (RANS) approach, since the length scale of the turbulence equals the length scale of the mean flow inhomogeneity. Kuehlert et al. (2008) report reasonable agreement with the experimental data for the velocity field, for both LES and RANS approaches. Nevertheless, LES exhibits clearly a better comparison for turbulence kinetic energy, which has a significant impact on heat transfer.

Hassan and Barsamian (2004) performed also a LES analysis of the experiments reported by Simonin and Barcouda (1988). They argue that the periodic separation of eddies from the cylinders results into an unsteady flow, which induces vibrations on the structures. It is observed that the highest pressure gradients are obtained at the top of the bundle, between the tubes and the wall. While the pressure is relatively constant in the passages between tubes, it fluctuates in the wake of the bundle and at the impact zones. Vortex shedding is observed in the wake of the bundle. The rotating structures, which separate in the shedding region, are transported by the flow from regions of low velocity to regions of high velocities.

Benhamadouche and Laurence (2003) performed a comparison of the transient RANS and LES. For both approaches, acceptable agreement is reported for coarse meshes (for coarse LES 99% of the cells have $y^+ < 11$). This finding suggests that the dominant turbulent structures are large enough to be captured satisfactorily even with meshes suitable for engineering purposes. The LES results are slightly more consistent with a DNS benchmark data than the transient RANS (employing the Launder, Reece and Rodi - Reynolds stress turbulence model – LRR RS TM). Severe overestimation of the total Reynolds stresses and unrealistic strong vortex shedding is reported for 2D simulations (transient RANS with LRR TM).

Considering the numerical treatment needed to solve adequately the flow through a pipe bundle, the major drawbacks imputed to the eddy viscosity TMs are their inability to capture the turbulent

anisotropy, poor prediction of the stresses in the wake region and of the vortex-shedding pattern. While some authors report rather good results for the prediction of the velocity field, the turbulent kinetic energy remains an issue. Based on the reported remarks and considering the engineering tasks in the present study, the flow through the pipe bundle has been treated by transient RANS using Reynolds-stress TMs.

1 ELSY NUCLEAR REACTOR

At nominal design conditions, the ELSY reactor estimated thermal power is about 1500 MW at a total lead mass flow rate of 129.12 tons/s.

The main advantages offered by the employment of lead as primary coolant are its good thermal properties, low chemical activity in contact with air and water (no explosion danger), low moderation rate, and acceptable costs. The main drawbacks are its high solidification temperature (327 °C), rather high oxidation and corrosion effects, and the reduced operation experience with lead.

The compact design (see Figure 1) proposes that the reactor vessel will contain the core, the control rods and their drive mechanism, all eight heat exchangers with their corresponding primary pumps, four decay heat removal (DHR) systems, and the Reactor Vessel Air Cooling System (RVACS) cooling system. The RVACS system is located between the reactor vessel and the concrete support of the reactor. The task of the system is to transfer by natural circulation into the atmosphere part of the heat dissipated by the core. The HXs and DHR HXs are distributed symmetrically around the core of the reactor. In each HX the pump is coaxially installed and has a rotational velocity of 140 rpm at nominal conditions.

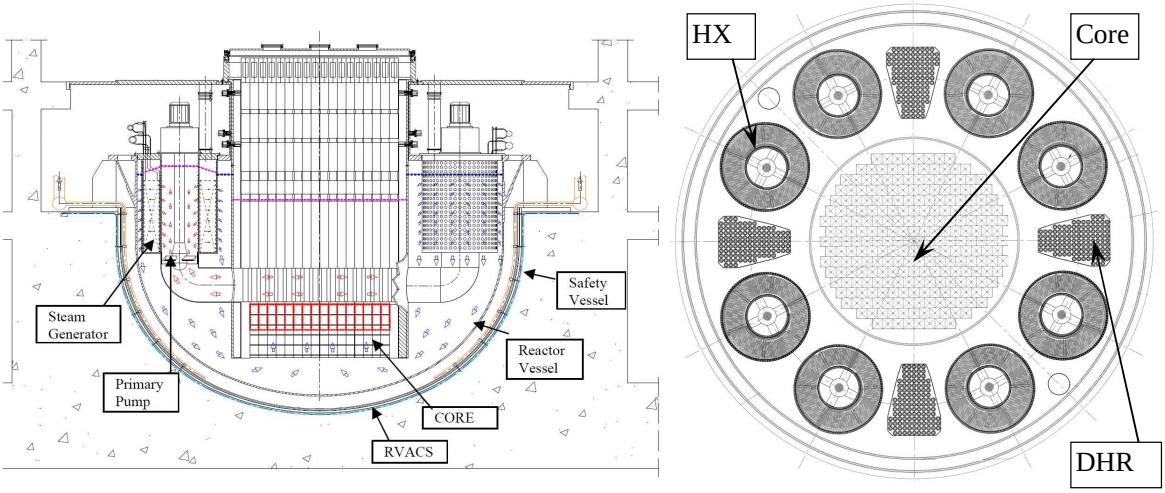

Figure 1 Vertical cut sketch of the ELSY RV (from Alemberti et al., 2009); Cross-section through the RV

Lead is employed for the primary circuit, while for the secondary circuit supercritical water is used. It is estimated that lead enters the core at about 400 °C and exists at approximately 480 °C.

The HX design is based on the "safety-by-design" approach described by Carelli et al. (2004). Potential issues that arise from the flow in the primary circuit out of the vessel are eliminated in the design stage, by placing the entire primary circuit in the RV. Furthermore, the next measures are considered to eliminate the risks of tube ruptures in the HX:

a) the water and steam collectors are placed outside of the RV, to prevent this low probability severe accident, which has catastrophic consequences;
b) check valve installation on each tube and Venturi nozzle on the feed water header, to inhibit the reverse steam flow, while any leakage is limited to choke flow;
c) in case of pressure surge in the HX due to a HX tube rupture, the mixture of water-steam-lead shall be forced to flow upwards, exiting the primary boundary and without risking to damage the reactor internals. For this purpose the lateral 50 mm thick inner and outer walls are doubled by perforated 5 mm thick companion shells (CS), placed on the bundle side, at a horizontal distance of 5mm. The CSs are held by spacers that are designed to collapse under certain pressure and since the

perforations in the CSs are staggered to the ones in the walls, the lateral flow will be inhibited (see inset in Figure 2).

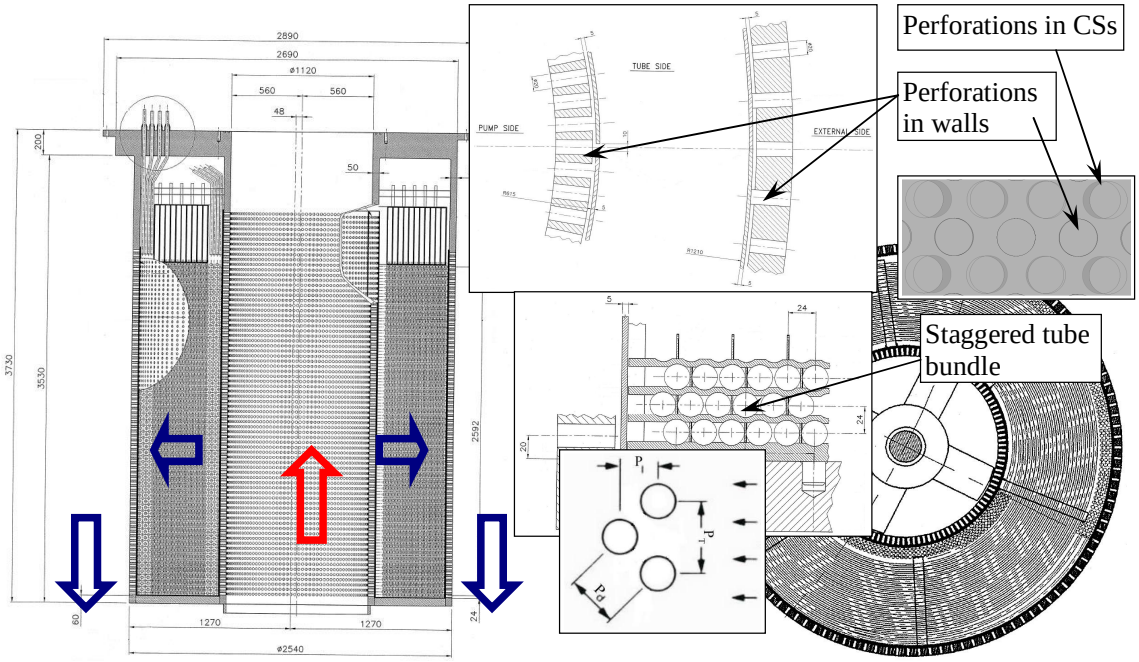

Figure 2 Sketches of cross-sections through the heat exchanger

The 76 vertical perforations on the inner wall (IW) are distributed on a height of 3 m and on a height of 2.7 m for the outer wall (OW). In circumferential direction, 118 perforations are uniformly distributed. All perforations have a hydraulic diameter of 20 mm. The HX is shown in a vertical cut and in cross-section in Figure 2. The pipe bundle, placed perpendicular to the HX axis, has all 218 spiral tubes arranged in a staggered way (see inset in Figure 2). The feed water pipes are placed on the OW side, while the steam outlet pipes are placed on the IW side. The supporting elements for the pipe bundle were not considered in the CFD models.

Table 1 Pitch-to-diameter ratios (see inset in Figure 2) for several experiments with staggered pipe bundles (Reynolds number based on the inlet velocity and pipe hydraulic diameter)

Experiment	**Reynolds number**	**D_h**	**P_t/D_h**	**P_d/D_h**	**P_l/D_h**
Aiba et al. (1982)	30 000	25	1.2	1.34	1.2
	40 000		1.6	1.79	1.6
Balabani and Yianneskis (1996)	12 858	10	3.6	2.41	1.6
Iwaki et al. (2004)	1 260-6 933	15	1.5	1.5	1.3
Konstantinidis et al. (2004)		10	3.6	2.77	2.1
Paul et al. (2007)	4 800-14 400	25.4	3.8	2.83	2.1
Simonin and Barcouda (1988)	18 000	21.7	2.07	1.47	1.04
ELSY Reactor (present study)	~21 250	22.22	2.16	1.21	0.54

An overview of the pitch-to-diameter ratios for some pertinent experiments found in literature is given in Table 1. The transversal pitch P_t is the vertical distance between two neighbouring tubes, the diagonal pitch P_d is the diagonal distance between two staggered neighbouring tubes and the longitudinal pitch P_l is the distance between two staggered tubes in radial flow direction (see inset in Figure 2). The ELSY design exhibits the most compact geometry, having the smallest pitches in longitudinal and diagonal directions. The experiments performed by Simonin and Barcouda (1988)

match best the geometry and flow conditions in the present study. Nevertheless, the P_l/D_h ratio differs by a factor of about 2. According to the results of Aiba et al. (1982) an unsteady flow field is expected for a tight pipe arrangement having a $P_l/D_h < 1.2$. Since the longitudinal pitch in the present study is a factor 2.2 smaller, strong flow instabilities are expected.

2 RESULTS AND DISCUSSION

The pressure loss has been determined using Bernoulli's law, considered between locations A and B:

$$\Delta P = \left[\underbrace{\rho v^2/2}_{\text{dynamic pressure}} + \underbrace{\rho g h}_{\text{hydraulic pressure}} + \underbrace{p}_{\text{static pressure}} \right]_A - \left[\rho v^2/2 + \rho g h + p \right]_B \quad (1)$$

where ΔP is the pressure loss, v is the mean velocity, ρ is the mean density, h is the height difference and p represents the static pressure. The law can be used along continuous streamlines, for flows with no viscous effects and constant densities.

The relevant parameter for flows exhibiting vortex shedding is the Strouhal number:

$$St = \frac{f\,D}{V_\infty} \quad (2)$$

where f is the frequency of the vortex shedding and V_∞ is the free stream velocity. For tube arrays the Strouhal number is based on the tube diameter and average flow velocity at the minimum cross-section between tubes (Blevins, 1977), which is the diagonal space between tubes for ELSY project. Based on the data presented by Blevins (1977), who cites the work of Fitz-Hugh (1973), the Strouhal number is estimated to be St ~ 0.95.

For an array of tubes in which the vortex shedding pattern is complex, the Strouhal number is much larger than for a single cylinder. As discussed by Zukauskas and Ulinskas (1990) St decreases up to 50% with increasing Reynolds number. The flow instabilities in an array of tubes result in a strong variation of the local velocities, consequently affecting St. Results presented by Zukauskas and Ulinskas (1990) suggest that the Strouhal number decreases continuously with increasing transversal and longitudinal pitches, P_t/D and P_l/D, until it reaches a constant value. For a constant transversal pitch, the Strouhal number decreases sharply with increasing longitudinal pitch. This leads to the expectation of a rather high value of the Strouhal number for the present study, since the P_l/D ratio is very small (see Table 1).

Weaver et al. (1993) report Strouhal values for different diagonal pitches (and based on the flow velocity upstream of the tubes). They conclude that, except for one diagonal pitch ratio, the experimental data fit two curves, corresponding to the first and second tube rows. The pitch ratio for which only one frequency is detected is equal to the ratio of the ELSY bundle, namely $P_d/D = 1.21$. For this pitch ratio, the Strouhal number reported is 1.94, which is twice the value reported by Fitz-Hugh (1973). Weaver et al. (1993) consider the experimental results of Fitz-Hugh (1973) of limited use due to the scatter data that is attributed to inconsistent methods of measurement, experimental error or to the existence of multiple Strouhal numbers, since the parameter is dependent on the Reynolds number. The frequency of vortex shedding should be compared to the natural frequency of the tubes and with the fluid acoustic frequency, in order to avoid the vibrations caused by a possible resonance.

2.1 Validation of the numerical models for pressure loss calculations

In a previous study (Onea et al., 2010) we report the qualification of our CFD models for pressure loss calculations through pipe bundles against the empirical prediction proposed by Gaddis and Gnielinski (1997). The Speziale, Sarkar and Gatski (SSG) Reynolds-stress TM is recommend over eddy-viscosity TMs, mainly due to the ability of handling the anisotropy of the turbulent structures. The numerical results obtained for pressure loss are within the accepted validity range of ± 35%.

No empirical predictions for pressure loss through double walls having staggered perforations have been found in literature. Therefore, the correlations proposed by Idelchik (1986) and Stichlmair (2006) have been considered in order to validate the CFD models for pressure loss calculations. Both authors discuss the case of one contraction in a channel, while the former one considers also a plate having multiple uniform vertical perforations.

The pressure loss for a channel with contraction has been derived by Idelchik (1986) and Stichlmair (2006) in a similar form:

$$\Delta P = \zeta \frac{\rho w_h^2}{2} \tag{3}$$

where w_h represents the mean velocity in the perforation and ζ is the coefficient of pressure loss. Idelchik (1986) uses in Equation (3) for both cases the mean velocity in the tube w_1, downstream of the perforation, instead of the mean velocity in the perforation w_h, which was used by Stichlmair (2006). Since the correlations in Idelchik (1986) are valid for $Re = w_h d_h / \nu > 10^5$, while the Reynolds number based on w_h and d_h for the ELSY geometry is about 62 000, the relations proposed in Idelchik (1986) should be treated with caution. From the mass balance the mean hole velocity is $w_h = 0.546$ m/s and the mean channel velocity is $w_1 = 0.137$ m/s. The results are summarized in Table 2.

Table 2 Pressure loss for perforated plates. Comparison between the theoretical predictions and CFD models

	Tube with contraction (Stichlmair; 2006)	Tube with contraction; perforated plate (Idelchick; 1986)	ANSYS CFX	
			Coarse grid	Fine grid
Coeff. pressure loss ζ_0 [-]	1.47 ÷ 1.57	0.9375		
Coeff. pressure loss ζ [-]	1.0325 ÷ 1.1325	15.8		
Pressure loss [bar]	0.01616 ÷ 0.01773	0.01546	0.0178	0.017
Deviation [%]	Reference	-	5	0.7

The CFD models consider a long pipe having a contraction in the centre. The length of the pipe before and after the contraction is about 30 times larger than the hydraulic outer diameter of the pipe, in order to allow the flow to develop. The diameter and length of the contraction correspond to one hole in the ELSY inner wall, namely the inner diameter is d_h = 20 mm and D_h = 40 mm. For the mesh construction, the recommendations given by Erdal and Andersson (1997) have been considered, especially in the region of the contraction. Therefore, the thickness of the first cell upstream the contraction was set to $0.001 \times D_h$. The coarse mesh has 4.9 million cells (80 cells in radial direction), while the fine mesh has almost 9.2 million cells (140 cells in radial direction). At the walls, no slip boundary conditions have been employed. All simulations have been performed with the SST TM. The results are compared in Table 2 against the empirical correlations previously mentioned.
The flow exhibits a typical behaviour, namely a rather small bottleneck effect at the beginning of the contraction and the toroidal vortex after the contraction. The pressure loss for the CFD model has been considered at positions with no streamwise pressure gradient (and not influenced by the hole), namely at the inlet and close to the outlet of the model. The deviation between the CFD models and the arithmetic averaged value of the pressure loss determined with relation (3) is 5% for the coarse model and less than 1% for the fine model, as displayed in Table 2. Therefore, it can be concluded that the CFD model is qualified for pressure loss simulations. Accordingly, it can be stated that the employment of a small radial cell is of significant importance.

2.2 Detailed local approach

The first approach considers a unit slice that consists of one hole in circumferential direction (i.e. a 3° arc), and three vertical holes in the IW and OW. For this configuration, five horizontal layers of pipes fit into the model. We mention that the pipes have not a spiral form, but follow the shape of a circle arc. This aspect has no influence on the pressure loss, but simplifies the construction of the model. Since no uniform and periodic flow patterns were observed during a run for 3 s, the final transient runs were restricted to 1.5 s, with data being saved every 0.1 s. Based on the results from Onea et al. (2010), the time step was set to 0.005 s, in order to keep the Courant number under 5 (see Table 3). Two mesh sizes were tested, the coarse one having 2.77 million cells, while the fine one has 5.27 million cells. The hexagonal unit cell grids used to discretize the tubes are shown in Figure 3. They consist of 10 cells for the coarse mesh and 18 cells for the fine mesh in radial direction, while in circumferential direction the tubes are discretized by 48, respectively 88 cells. The main recommendations proposed by OECD/NEA (2007) for the mesh construction have been respected.

For the walls, the largest part of pressure loss occurs in the narrow gap between the walls and the CS, where the flow is forced to split in four and make two 90° turns in the diagonal path between the holes in the wall and CS. In the present paper, we will not focus on the flow through the walls, since this discussion was already made in our previous study (Onea et al., 2010), where the flow characteristics through the IWs were analyzed.

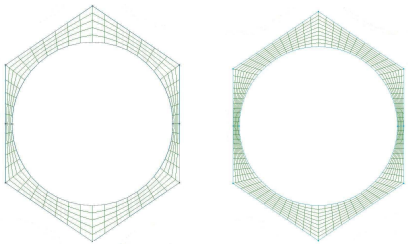

Figure 3 Coarse/fine mesh around tubes

The flow through the pipe bundle is unsteady. In Figure 4 the time dependent velocities are displayed for relevant points in the bundle. The jet coming from the IW is slightly oscillating in time (Point 1) and has the largest velocity. The lowest velocity is encountered in the region between the IW and bundle (Point 2), where chaotic vortices are created. The velocities in the pipe bundle have almost the same magnitude, but at the outlet of the pipe bundle (Point 5) the velocity is slightly smaller due to the divergent shape of the model and frictional losses. The velocity fluctuations are chaotic in time and no clear time evolution of the profiles could be established, even if a longer time period was considered. The flow follows a sinuous path in the passages between two vertically neighbouring layers of pipes (see velocity streamlines in Figure 5). In Figure 6 are displayed the time-averaged velocities in cylindrical coordinates for relevant vertical lines placed in the bundle (at entrance, centre, and exit). The dominant flow in the bundle is in radial direction. The flow exhibits fluctuations even before contacting the first row of tubes, due to the unsteady vortices developed between the inner CS and the pipe bundle. This behaviour is confirmed by the negative radial flow encountered at the first tube row (see velocities for line 1 in Figure 6). The jet-type flow at the CS holes contributes also to the generation of these vortices. Nevertheless, the growth of these vortices will be prohibited in a real design due to the presence of the vertical outlet pipes, which were not considered in this model. The vortices created between the CS and the pipe bundle induce an asymmetry of the axial velocity (vertical direction) at the first contact of the main sinuous flow with the first staggered tube row (see velocities along line 2 in Figure 6).

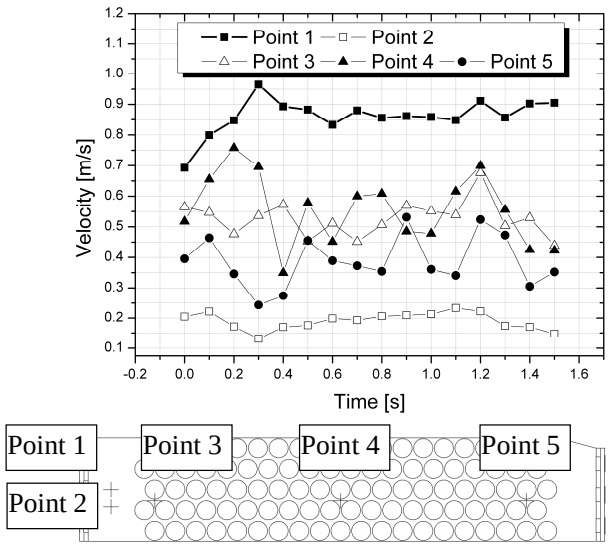

Figure 5 Time series of velocities at shown points (SSG RS)

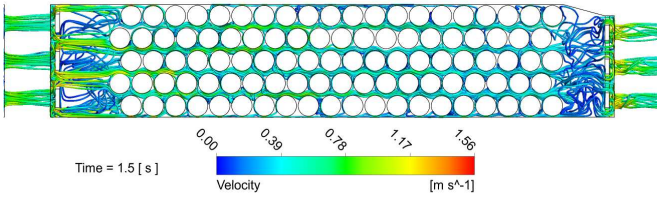

Figure 4 Instantaneous velocity field through the detailed unit slice model (SSG RS)

At the flow contact region with the tubes, the flow is accelerated, leading to strong velocity gradients in the boundary layers. The lead flow behaves as a high velocity jet. It can be observed that the radial velocity profiles have a U-type shape, due to the presence of the next row of staggered pipes. The peaks in the radial velocity are encountered rather equidistantly, as it is also reported in Iwaki et al. (2004). Nevertheless, the time averaged peaks in the radial velocity vary in the pipe bundle in the range of 0.3 ÷ 0.6 m/s, while in the mentioned study they are constant. The flow has a pulsating behaviour due to the tight longitudinal arrangement of the pipes (low P_l/D_h). Generally, it can be stated that the axial velocity has larger fluctuations than the circumferential velocity. In the first half of the pipe bundle flow structures at the upper side of the bundle tend to flow downwards, while flow structures at the

bottom part tend to flow upwards (see results along lines 2 and 4). This pattern is attributable to the model delimitations in height.

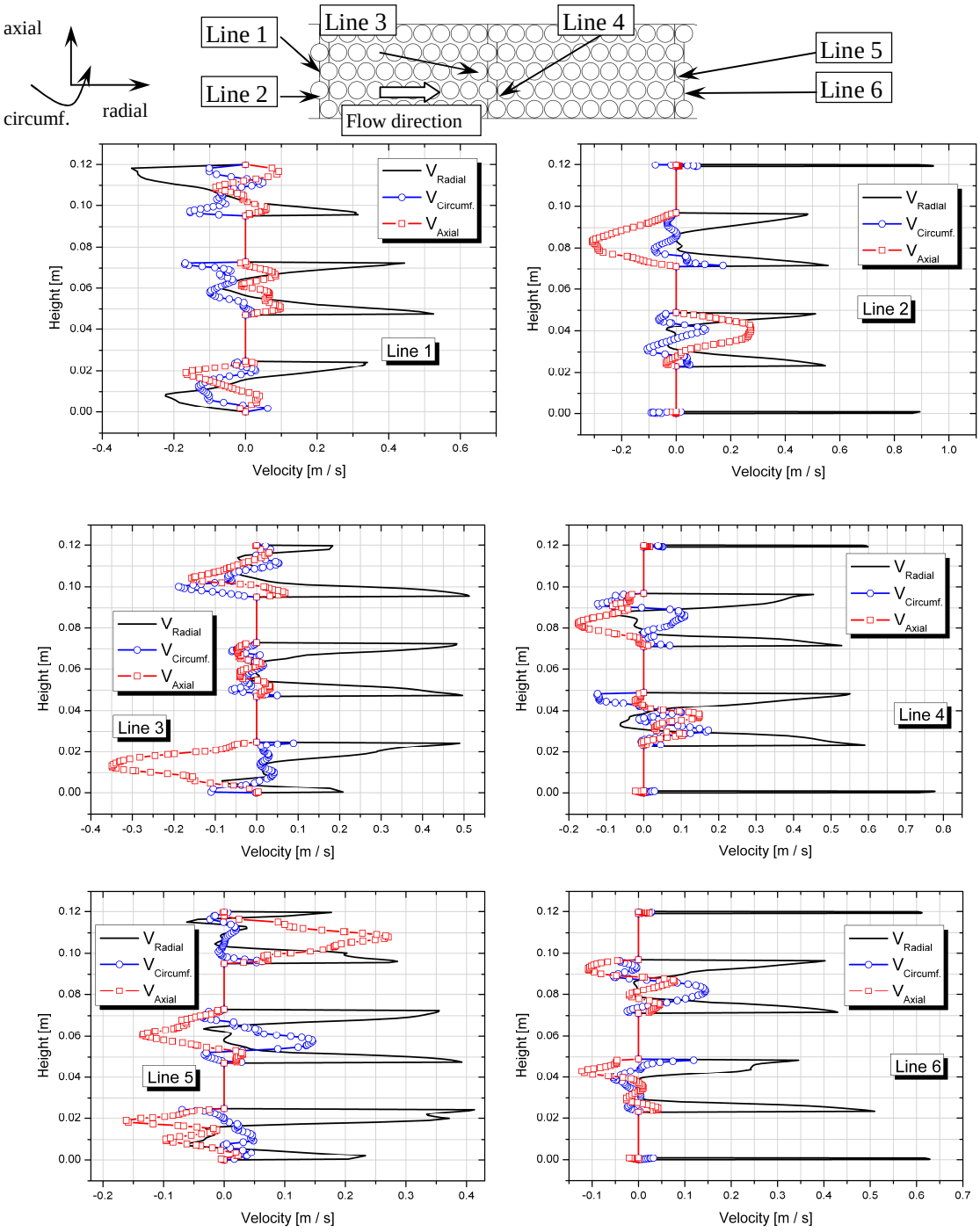

Figure 6 Time-averaged velocity profiles (cylindrical coordinates) along vertical lines at entrance, centre and exit of the pipe bundle

In the typical pipe bundle studies in literature, the shedding of vortices in the tube wake is observed. In the present design, the dense pipe arrangement allows physically no room for vortex shedding in the tube wake. Therefore, the flow structures are reflected by the horizontal pipe layers, giving birth to a pulsating main radial flow and creating fluctuations in the flow. The complex interaction between the main sinuous radial flow in the passage between pipe layers and the reflected vortices leads locally to partial blockages of the flow. In these regions, the flow is partially diverted towards vertically

neighbouring flow passages. Hence, the velocity fluctuations in the axial velocity are larger than for the circumferential velocity. Vortices are also generated due to the flow deviations and contact with the pipe walls. Another source of flow asymmetry is the fact that the lead enters the pipe bundle not as a uniform vertical field, but in a jet form, generated by the holes in the CS.
Between the IW and OW the pressure loss was calculated using Bernoulli's law (1). The values calculated differ less than 0.5 % in comparison to the pressure difference determined at the same locations. As seen in Table 3, the total pressure loss for the coarse grid is about 4 % smaller than for the fine grid, which is a satisfactory result for engineering purposes. Three turbulence models have been tested. The SSG Reynolds-stress TM is able to capture the flow turbulent anisotropy and it is recommended over eddy-viscosity TMs for flows in pipe bundles. The Baseline Explicit Algebraic Reynolds-stress (BSL-EARSM) TM considers a nonlinear relation between the Reynolds stresses, the mean strain-rate, and the vorticity tensors. The model is based on the standard k-ε and Baseline (BSL) TMs and it is recommended for cases exhibiting secondary flows and strong streamline curvatures (ANSYS CFX, 2009). The Scale Adaptive Simulation (SAS-SST) TM is based on the eddy-viscosity SST TM by introducing the von Karman length-scale into the turbulence scale equation. By means of a blending function, the model switches between LES behaviour in the unsteady regions and RANS (SST) behaviour in the stable regions. The time step requirement for the model is rather strict, i.e. Courant number < 1. Both Reynolds-stress TMs gave the same results for the pressure loss, while the SAS-SST predicted a pressure loss about 8.6 % larger, an acceptable value considering the fact that the Courant number was slightly larger than the model requirement.
In the present study, we do not claim to solve the heat transfer issue between the primary and secondary sides, since our main interest was the flow hydrodynamics. Therefore, our approach for the heat transfer is rather simple. In our previous study (Onea et al., 2010), the calculation has been considered isothermal (average temperature of 400 °C), in contrast to the present simulations, where the tubes temperature was set to the mean value of 440 °C. The lead temperature was set to 480 °C at the inlet and to 400 °C at the outlet. Therefore, the total pressure loss determined in this study is slightly smaller than the one reported in Onea et al., 2010.
For the SSG RS TM, the time averaged pressure losses estimated with Bernoulli's law for each major component are 0.108 bar for IWs, 0.11 bar for the pipe bundle and 0.076 bar for the OWs. The results are in excellent agreement with the pressure losses estimated using models that have treated each component separately and reported in our previous study.

Table 3 Pressure loss for the unit slice CFD models

Grid size [mil. cells]	2.77 (coarse)	5.27 (fine)	5.27 (fine)	5.27 (fine)
Turbulence model	SSG RS	SSG RS	BSL-EARSM	SAS-SST
Pressure loss^{IW-OW} [bar]	0.290	0.303	0.303	0.329
Tubes mean y^+ [-]	56.8	37.5	36.3	34
Courant number [-]	4.02	3.63	3.26	3.72

For both meshes, the distribution of the y^+ has a similar pattern. The y^+ magnitude lies in the viscous sub-layer ($y^+ < 5$) at the lateral front side (that corresponds to the stagnation points) and lateral back side of the tubes. On the upper and bottom regions of the tubes, the y^+ magnitude reaches the log-law domain ($y^+ > 60$), but are in general smaller than 120 (fine mesh). The largest mean y^+ values are encountered on the first row of cylinders, on the upper and bottom regions. In streamwise direction, the tube upper and bottom areas corresponding to the log-law region decrease continuously in a significant manner, in parallel with the decrease of the maximum y^+ peaks. The maximum local y^+ peaks reach about 200 for the fine mesh and about 300 for the coarse mesh. The time averaged y^+ values are summarized in Table 3. The time averaged y^+ for the coarse mesh is about 50 % larger than for the fine mesh. Nevertheless, the influence on the pressure loss is rather negligible.

2.3 Simplified global approach

A simplified model of the entire HX has been considered, in order to determine the total pressure loss and to account for the rotating jet generated by the pump. The velocity field considered at the entrance in the HX has been issued from the CFD analysis of the pump, using a model developed by Ansaldo

Nucleare (Corsini, 2008). Since the pump analysis considered a steady-state approach, the velocity field was averaged in space. The SSG Reynolds-stress TM was employed for the CFD analysis of the pump.

For the simplified global model, the IWs, the OWs and the pipe bundle were not considered in a detailed geometrical manner, but structured uniform domains were used to emulate their presence (see mesh in Figure 7 b). Directional losses were implemented within these sub-domains. The streamwise resistance loss coefficients ζ were determined using Equation (3) and considering the pressure losses determined in Onea et al. (2010), namely 0.103 bar for the IW, 0.1 bar for the pipe bundle, and 0.078 bar for the OW. The transversal losses were set accordingly, namely 100 (IW), 100 (pipe bundle) and 150 (OW) times larger than the streamwise loss coefficient. Within these domains, the lead was allowed to flow only in radial direction, as can be seen in Figure 7 b). An extended domain was considered to enclose the HX, to allow the lead to flow downwards. The TMs considered are SSG RS and BSL RS. For the temperature field, the inlet was set to 480 °C, the outlet to 400 °C, while in the pipe bundle region a heat sink was considered. The total pressure loss determined by Bernoulli's law applied between the horizontal inlet surface and the corresponding horizontal surface from the extended domain (light blue surface in Figure 7) is 0.50 bar (SSG RS), respectively 0.49 bar (BSL RS). Nevertheless, the pressure losses for each main component are slightly larger than the losses estimated with the detailed local models, due to imperfect setting of the loss coefficients. Extracting the differences to the detailed local models, the pressure loss in this simplified global model reaches about 0.43 bar (SSG RS), respectively 0.41 bar (BSL RS).

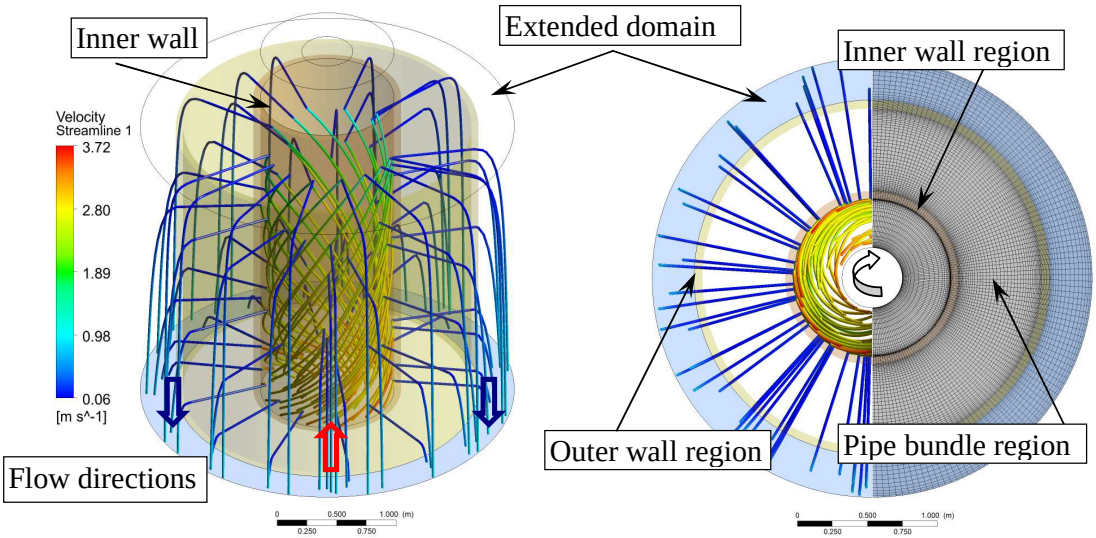

a) Isometric view b) Model cross-section (mesh view)

Figure 7 Velocity streamlines and mesh visualisation for the simplified complete HX model

The pressure loss determined with Bernoulli's law between the horizontal HX entrance and the vertical IW is 0.116 bar (SSG RS) and 0.102 bar (BSL RS). This pressure loss is caused physically by the energy lost in the generation of the lead swirl by the pump. Summing this pressure loss and the pressure loss determined for the major components (IW, pipe bundle, and OW) in the previous section, namely 0.303 bar, a pressure loss of about 0.42-0.43 bar is estimated.

The flow is represented by streamlines in Figure 7. The pump, which is situated just below the entrance in the HX, generates a swirl in the region enclosed by the IWs. In this cylindrical region, the axial velocity decreases relatively strongly in magnitude along the height of the HX, as displayed in Figure 8, where the velocity distribution between the pump shaft and the IWs is shown. A recirculation zone is developing inside the swirl, on the pump shaft side, due to the centrifugal force that pushes the lead towards the IW, thus creating a "void" on the shaft side. The circumferential velocity decreases significantly below this inner vortex. The radial velocity has a peak at the entrance into HX, decreases constantly near the IW and fluctuates around zero in the inner recirculation region. Since there are no perforations on the upper part of the IW a vortex is formed in that region.

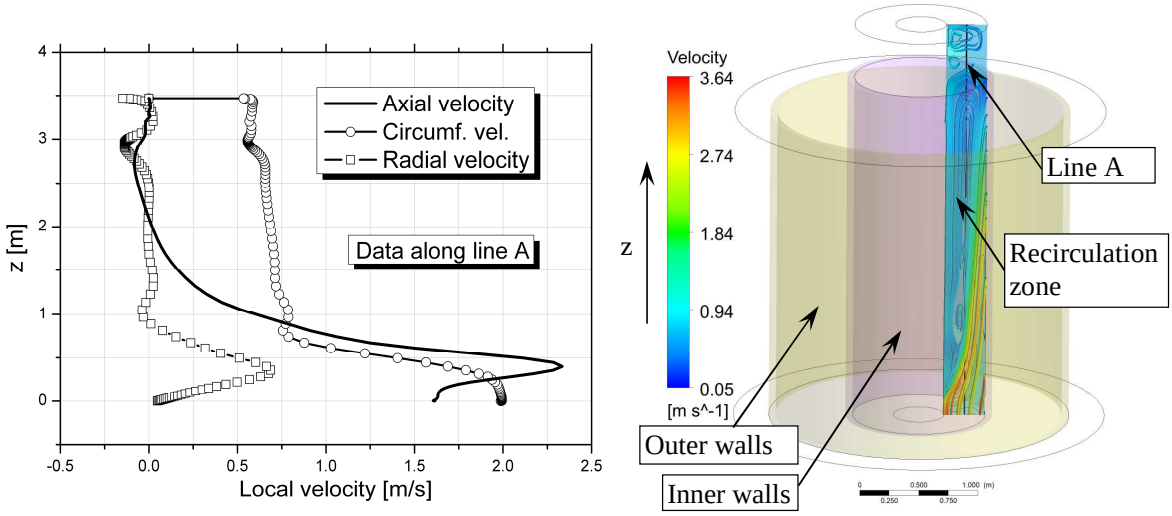

Figure 8 Velocity distributions along the height of the heat exchanger

The flow pattern implies that, for the region between the pump shaft and the IW, the largest part of the mass flow will stream through the bottom part of the HX. The flow in the bottom part has a larger circumferential component and a larger magnitude than the flow in the upper region. Therefore, the holes in the IW will be streamed vertically in a slight non-uniform manner.

3 CONCLUSIONS

The present study focuses on the estimation of pressure loss through the HX of the ELSY nuclear reactor project. A detailed approach by using unit slice models and a simplified global approach have been considered. For the former approach, the pressure loss determined is about 0.3 bar, which represents the pressure loss in the major components of the HX. Considering also the entire swirl generated by the pump, at the entrance in the HX, by means of the second approach, the pressure loss for the entire HX is estimated to be about 0.41-0.43 bar.

At nominal conditions, the accepted values for pressure loss in the primary circuit are about 0.9 bar in the reactor core, 0.5 bar in the HX and 0.25 bar in the upper plenum and in the pumps. The total pressure loss in the primary circuit is therefore estimated at 1.65 bar. Accordingly, it can be stated that the pressure loss estimated for the HX is below the requirements issued in the design.

It should be mentioned that other sources of additional pressure loss still have to be considered, e.g. the pipe supports and other mechanical elements that were not considered in the study.

ACKNOWLEDGEMENT

The authors acknowledge the efforts of all scientists that participated in the ELSY project. The financial support offered by the European Commission is also appreciated. The help received from Fabrizio Magugliani and Alessandro Alemberti (Ansaldo Nucleare), for providing the data from the pump analysis, is also acknowledged.

REFERENCES

S. Aiba, H. Tsuchida, T. Ota, “Heat transfer around tubes in staggered tube banks”, *Bulletin of the JSME* 25, 204, 927 – 933, (1982)

A. Alemberti, J. Carlsson, E. Malambu, A. Orden, L. Cinotti, D. Struwe, P. Agostini, “European lead fast reactor”, *Proc. 7th Europ. Comm. Conf. Euratom Res. Training in Reactor Systems*, Prague, Czech Republic, 22-24 June, 2009

ANSYS CFX, Release 12, “*Solver User Guide*”, 2009

S. Benhamadouche, D. Laurence, “LES, coarse LES, and transient RANS comparisons on the flow across tube bundle”, *Int. J. Heat Fluid Flow* 24, 470-479 (2003)

M. Böttcher, A. Onea, "CFD primary loop analysis of the ELSY reactor with focus on decay heat removal", *Proc. Annual Meeting on Nucl. Tech.*, paper no. 1207, Berlin, Germany, 4-6 May, 2010

R. D. Blevins, *Flow-induced vibration*, Van Nostrand Reinhold Company, New York, USA, 1977

M. D. Carelli et al., "The design and safety features of the IRIS reactor", *Nuclear Eng. and Design*, 230, 151 -167 (2004)

G. Corsini, "Primary pump design report and drawing", ELSY Report DEL/08/017, Ansaldo Nucleare (confidential), 2008

A. Erdal, H. I. Andersson, "Numerical aspects of flow computation through orifices", *Flow Meas. Instrum.* 8, 1, 27-37 (1997)

J.S. Fitz-Hugh, „Flow induced vibration in heat exchangers", Oxford University Report RS 57, 1973

E.S. Gaddis, „Druckverlust in querangeströmten Bündeln aus glatten sowie berippten Kreis- und Ovalrohren", *VDI Heat Atlas 3.0*, Springer-Verlag, Berlin Heidelberg, 2006

E.S. Gaddis, V. Gnielinski, Verfahrenstechnik 17, 7, 410-418 (1983)

E.S. Gaddis, V. Gnielinski, "Pressure drop on the shell-and-tube heat exchangers with segmental baffles", *Chemical Engineering and Processing* 36, 149-159 (1997)

Y.A. Hassan, H.R. Barsamian, "Tube bundle flows with the large eddy simulation technique in curvilinear coordinates", *Int. J. Heat Mass Transfer* 47, 14-16, 3057-3071 (2004)

I.E.Idelchik, *Handbook of hydraulic resistance*, 2nd edition, Hemisphere Publishing Co., 1986

C. Iwaki, K. H. Cheong, H. Monji, G. Matsui, "PIV measurement of the vertical cross-flow structure over tube bundles", *Experiments in Fluids* 37, 350-363 (2004)

K. Kuehlert, S. Webb, D. Schowalter, W. Holmes, A. Chilka, S. Reuss, „Simulation of the fluid-structure-interaction of steam generator tubes and bluff bodies", *Nucl. Eng. Design* 238, 2048-2054 (2008)

E. Konstantinidis, S. Balabani, M. Yianneskis, "Phase-average mean flow and turbulence structure in a staggered cylinder array subjected to pulsating cross-flow", *J. Fluids Eng.* 126, 323 – 336 (2004)

W. Ma, A. Karbojian, B.R. Sehgal, T.-N. Dinh, "Thermal hydraulic performance of heavy liquid metal in straight-tube and U-tube heat exchangers", *Nucl. Eng. Design* 239, 1323-1330 (2009)

OECD/NEA-6195, *Handbook on lead-bismuth eutectic alloy and lead Properties, materials compatibility, thermal-hydraulics and technologies*, ISBN 978-92-64-99002-9, 2007

A. Onea, M. Böttcher, D. Struwe, "Detailed CFD analysis of the pressure loss on the primary side of the heat exchanger for the ELSY fast lead-cooled reactor by applying unit slice models", *Proc. ASME-ATI-UIT Conference on Thermal and Environmental Issues in Energy Systems*, vol. II, 1463-1468, Sorrento, Italy, 16-19 May, 2010

S.S. Paul, M.F. Tachie, S.J. Ormiston, "Experimental study of turbulent cross-flow in a staggered tube bundle using particle image velocimetry", *Int. J. Heat Fluid Flow* 28, 441-453, 2007

W. Rodi, "Comparison of LES and RANS calculation of the flow around bluff bodies", *J. Wind Eng. Aerodynamics* 69-71, 55-75 (1997)

P. Rollet-Miet, D. Laurence, J. Ferziger, "LES and RANS of turbulent flow in tube bundles", *Int. J. Heat Fluid Flow* 20, 241 – 254 (1999)

O. Simonin M. Barcouda, "Measurements and prediction of turbulent flow entering a staggered tube bundle", *Proc. 4th Intern. Symposium on Applications of Laser Anemometry to Fluid Mechanics*, Lisbon, Portugal, 1988

OECD/NEA, "Best practice guidelines for the use of CFD in nuclear reactor safety applications", NEA/CSNI/R(2007)5, 2007

J. Stichlmair, „Druckverlust bei der Durchströmung von Lochplatten", *VDI Heat Atlas 3.0*, Springer-Verlag, Berlin Heidelberg, 2006

D. Sumner, S. J. Price, M. P. Païdoussis, "Flow-pattern identification for two staggered circular cylinders in cross-flow", *J. Fluid Mech.* 411, 263 – 303 (2000)

J.K. Watterson, W.N. Dawes, A.M. Savill and A.J. White, "Predicting turbulent flow in a staggered tube bundle", *Int. J. Heat Fluid Flow* 20, 6, 581-591 (1999)

D.S. Weaver, H.Y. Lian, X.Y. Huang, "Vortex shedding in rotated square arrays", *J. Fluids Structures* 7, 107 – 121 (1993)

A. Zukauskas, R. Ulinskas, "Banks of plain and finned tubes" in *Handbook of Heat Exchanger Design*, Hemisphere Publishing, Ed. G.F. Hewitt, Section 2.2.4, 1990